Bull Mater Sci (2021) 44:28
https://doi.org/10.1007/s12034-020-02277-2

A facile synthesis of g-C_3N_4/$BaTiO_3$ photocatalyst with enhanced activity for degradation of methylene blue under visible light

VAN KIM NGUYEN[1], VIET NGA NGUYEN THI[2], HUU HA TRAN[1], THU PHUONG TRAN THI[1], THANH TAM TRUONG[1] and VIEN VO[1,*]

[1]Department of Chemistry, Quy Nhon University, Quy Nhon City 820000, Vietnam
[2]Department of Education, Quy Nhon University, Quy Nhon City 820000, Vietnam
*Author for correspondence (vovien@qnu.edu.vn)

MS received 7 April 2020; accepted 2 July 2020

Abstract. g-C_3N_4/$BaTiO_3$ composite was hydrothermally synthesized at 200°C for 24 h from a dispersed mixture of g-C_3N_4 and $BaTiO_3$ in water, in which $BaTiO_3$ was hydrothermally synthesized at 200°C for 48 h using barium nitrate, isopropanol, titanium tetrachloride and sodium hydroxide as precursors without assistance of any surfactant; and graphitic carbon nitride (g-C_3N_4) was prepared by pyrolysis of melamine at 520°C. The obtained materials were characterized by X-ray diffraction, infrared spectra, scanning electron microscopy, elemental mapping, X-ray photoelectron spectroscopy and ultraviolet–visible diffuse reflectance spectroscopy. The photocatalytic activity of the materials was assessed by degradation of methylene blue (MB) under visible light. The enhancement of photocatalytic activity of the g-C_3N_4/$BaTiO_3$ composite compared to the single components, g-C_3N_4 and $BaTiO_3$ was observed, which is attributed to the reduction of combination rate of photogenerated electron–hole pairs in the composite. The MB degradation over the composite was mainly attributed to the photoreduction process induced by the superoxide radical anions ($^{\bullet}O_2^-$) and hydroxyl radicals ($^{\bullet}OH$); and a mechanism was also proposed based on the heterojunction model from the two semiconductor components.

Keywords. $BaTiO_3$; hydrothermal synthesis; photocatalytic activity; methylene blue.

1. Introduction

Pollution of environment, in particular water resource, caused by organic contaminants is becoming a more and more severe issue in demand of water purification. Among various techniques to eliminate organic pollutants in water, such as functional filtering membrane, ionic exchange, adsorption on activated carbon and advanced oxidation processes [1–3]; photocatalysis as a representative case of the advanced oxidation processes has been attracting much attention of scientists due to its simplicity, low toxicity, high chemical stability and degradation efficiency [4]. Numerous reports on this topic have focussed on the oxide semiconductors, such as TiO_2, ZnO and WO_3 as photocatalysts [5–9]. However, they significantly work under ultraviolet (UV) light, therefore, modifications of these oxides or design of new materials which can work efficiently under visible light have been emerged.

Perovskite materials are recommended as highly potential photocatalysts based on its superior photoactivity with high content of crystalline defects and deformation which could provide more trapping sites preventing recombination of photoinduced electron–hole pairs [3,10]. Additionally, vacancies between cation and anion O^{2-} sites in these structures could accelerate adsorption of oxygen on cationic surface sites, facilitating following photocatalytic reactions [10]. Bimetal oxide perovskites with general formula of ABO_3, especially with B = Ti and A = Ca, Ba, Sr [11–13], were reported in application of different fields, of which barium titanate ($BaTiO_3$) is considered as photocatalyst for decomposition of organic pollutants in aqueous media [14,15]. However, $BaTiO_3$ is active only under ultraviolet light due to its wide band gap (~3.2 eV). In addition, photocatalysts with single phase normally possess high recombination rate of photogenerated electrons and holes, leading to reduce its photocatalytic activity [16]. Therefore, a number of strategies to overcome this issue have been reported, in which the construction of hetero-structured composites from $BaTiO_3$ and other narrow-band gap semiconductors has attracted much attention [16–18].

Recently, graphite-like carbon nitride (g-C_3N_4), a non-metal polymeric semiconductor, has emerged as a photocatalyst with several remarkable properties including strong photoreactivity, high chemical stability and reasonable band gap of 2.7 eV [19,20], leading to good degradation of organic contaminants in water, water splitting for hydrogen evolution under visible illumination [21,22]. Owing to its unique properties, g-C_3N_4 has been also considered as a

Published online: 12 February 2021

potential component to design heterostructured photocatalysts.

To the best of our knowledge, few works on $BaTiO_3$/g-C_3N_4 composites have been published [16–18]. In this work, we report a facile method to prepare $BaTiO_3$/g-C_3N_4 composite which performs significant enhancement in photodegradation of methylene blue (MB) under visible light and a photocatalytic mechanism was also proposed.

2. Experimental

2.1 *Chemicals*

Titanium (IV) chloride ($TiCl_4$, ≥99.9%), melamine ($C_3H_6N_6$, ≥99.0%), barium nitrate ($Ba(NO_3)_2$, ≥99.0%), methylene blue hydrate ($C_{16}H_{18}ClN_3S{\cdot}xH_2O$, ≥97.0%), sodium hydroxide (NaOH, ≥97.0%), isopropyl alcohol ($(CH_3)_2CHOH$, ≥99.5%) were purchased from Sigma Aldrich and ethanol (C_2H_5OH, ≥99.9%) was purchased from Samchun (South Korea). All chemicals were of reagent grade and used without further purification.

2.2 *Preparation of materials*

$BaTiO_3$ was prepared using the following procedure. An appropriate amount of $Ba(NO_3)_2$ was dissolved in 46.6 ml of distilled water until obtaining saturated solution (labelled as solution A). Solution B was separately prepared by adding 2 ml of $TiCl_4$ to 5.6 ml of isopropanol, to which 39 ml of ethanol was then added. Solution A was dropped into solution B and continuously stirred for 2 h before the addition of 10 ml of 10 M NaOH with stirring for one more hour. The obtained solution was transferred into a close-packed Teflon to keep at different temperatures of 180, 200, 220°C for 48 h. The collected solids were separated via centrifugation then rinsed by distilled water to pH 7. After drying at 80°C for 10 h, the as-prepared samples were denoted as BTO-*T*, where *T* is referred as synthesis temperature (°C) (*T* = 180, 200 and 220).

g-C_3N_4 was synthesized via thermal decomposition of melamine. In a typical synthesis, melamine (5 g) in a ceramic cup with a cover was heated at 500°C for 2 h and then at 520°C for 2 h more with a ramp of 10°C min^{-1}. The obtained solid was washed with diluted HCl solution, ethanol and water; and denoted as CN.

g-C_3N_4/$BaTiO_3$ composite was prepared using a facile hydrothermal treatment. Accordingly, a mixture of CN and BTO-200 (CN:BTO-200 = 1:10 in weight ratio) was ground in a mortal for 2 h till fine powder. The gained mixture was then well dispersed in distilled water by stirring for 4 h before treating hydrothermally at 200°C for 24 h. The precipitation was collected by centrifugation and rinsed by distilled water and ethanol, then dried at 80°C for 24 h. The final powder was denoted as CN/BTO-200.

2.3 *Characterization*

Powder X-ray diffraction (XRD) patterns were recorded on a D8 Advance X-ray diffractometer with CuKα radiation (λ = 1.540 Å) at 30 kV and 0.01 A. Infrared (IR) spectra were obtained using an IR-Prestige-21 spectrophotometer (Shimadzu), scanning electron microscopy (SEM) images were examined using Nova Nano SEM 450. X-ray photoelectron spectroscopy (XPS) was performed on an ESCALab spectrometer (Thermo VG, UK) with monochromated AlKα radiation and ultraviolet–visible diffuse reflectance spectroscopy (UV–Vis DRS) were carried out on a GBC Instrument−2885.

2.4 *Photocatalytic activity evaluation*

To evaluate photocatalytic activity, MB was selected as a target pollutant. For 200 ml of MB solution (50 mg l^{-1}), the prepared photocatalyst of 0.1 g was dispersed with stirring and then the solution was kept in dark condition for 1.5 h. The solution was then irradiated with visible light (using a 75 W–220 V lamp with a filter cutting UV rays). The degradation of MB was monitored by taking the suspension at intervals of 1 h. Each of the suspension was centrifuged to separate the catalyst from the MB solution. Subsequently, the degradation rate was calculated as a function of irradiation time from absorbance change at a wavelength of 663 nm using a UV–Vis spectrophotometer (Jenway 6800). The percentage of degradation for MB was calculated using the following equation:

$$\text{Degradation } \% = \frac{C_0 - C_t}{C_0} \times 100\%,$$

where C_0 and C_t are concentrations of MB at the initial and *t* times, respectively.

3. Results and discussion

Figure 1a shows the XRD patterns of BTO-*T* samples. It is seen that when heating at 180 or 220°C, the samples exhibit no diffraction related to $BaTiO_3$ structure. Meanwhile, the BTO-200 pattern with peaks at 22.22, 31.55, 38.9, 45.11, 51.02 and 66.02° corresponding to crystallite (100), (110), (111), (200), (210), (211) and (220) planes of the cubic structure of $BaTiO_3$ was observed [23,24]. Furthermore, the mean crystalline size of BTO-200 was estimated to be 45 nm based on the value of (110) plane diffraction using Scherrer equation [25]. These data demonstrate that among three investigated temperatures, heating at 200°C is the appropriate condition for the formation of $BaTiO_3$ phase. At 180°C, it may not have enough energy to form $BaTiO_3$, while 220°C is high, leading to collapse of the structure. The obtained results show that when varying reaction temperatures for the preparation of $BaTiO_3$, the condition at

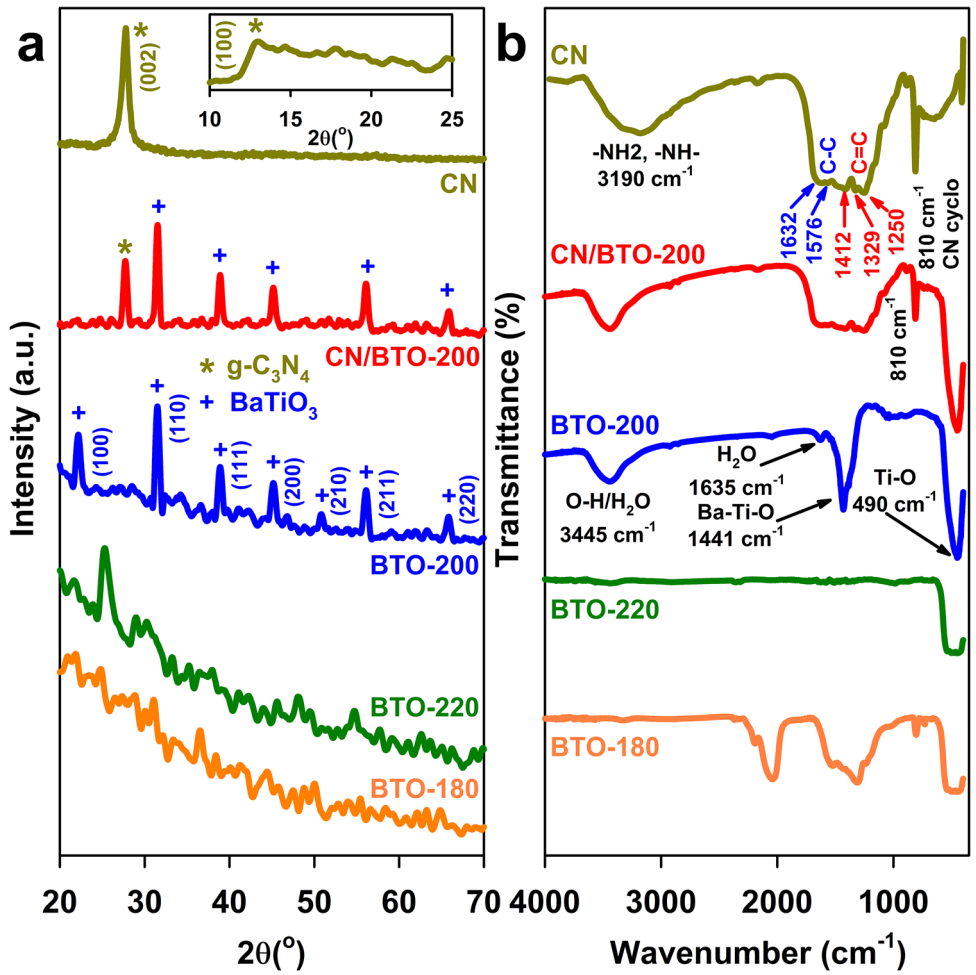

Figure 1. (**a**) XRD patterns and (**b**) IR spectra of BTO-180, BTO-200, BTO-220, CN and CN/BTO-200.

200°C is the best one. Therefore, BTO-200 was selected for latter investigations.

The XRD patterns of CN and CN/BTO-200 are also presented in figure 1a. For CN, the XRD pattern presents a strong peak at 27.3° and a weak peak at 13.2° (the inset) corresponding to (002) and (100) planes, respectively, which is consistent with the layered graphite-like structure of g-C_3N_4 [26,27]. In the case of CN/BTO-200, the pattern comprises both the diffraction systems of g-C_3N_4 and $BaTiO_3$ phase [23,24], which demonstrates a good combination of single components in the composite without any crystal structural changes.

For further investigation on structural bonding information, the IR spectra of as-prepared samples were conducted and the collected results are presented in figure 1b. For BTO-200, it is observed that a broaden band at 3445 cm^{-1} could be ascribed to the stretching vibration of O–H bonds of physically adsorbed H_2O molecules [28]. The peak at 1634 cm^{-1} could be assigned to bending vibration of coordinated water molecules [29]. The two strong peaks at 1441 and 490 cm^{-1} could be attributed to Ba–Ti–O and Ti–O, respectively [29,30]. These signals, however, could not be observed in the IR spectra of BTO-180 and BTO-220, which supports the above XRD data that heating at 180 or 220°C cannot form $BaTiO_3$ phase. For CN, it is observed that the peak at 810 cm^{-1} is attributed to the deforming vibration of triazine units [27], while the bands in the range of 1250–1412 cm^{-1} are ascribed to stretching vibration of C–N bonds, and C=N bonds are distinguished by the band of 1576–1632 cm^{-1} [27]. Additionally, vibration of primary amine (–NH_2) and secondary (–NH–) of triazine units in g-C_3N_4 are detected via a broaden band at around 3190 cm^{-1}. All the aforementioned signals characterized for the chemical interactions in structure of g-C_3N_4 and $BaTiO_3$, could be clearly observed in IR spectrum of CN/BTO-200, which further confirmed the co-existence of both phases in the composite. In detail, the bands at 810 cm^{-1} and in the region of 1250–1632 cm^{-1}, originated from g-C_3N_4 are observed [28]. Besides, the characteristic peak of Ti–O can be seen at 490 cm^{-1}, while the peak at 1441 cm^{-1} corresponding to the Ba–Ti–O bond [28–30] is not clear, which could be explained by the overlap of stronger vibrations of C–N or C=N in the same range.

The morphology of CN/BTO-200 was investigated using SEM technique. Figure 2a shows uniform spherical particles with diameter of ~50 nm, stacking together. Distribution of the components in CN/BTO-200 was also investigated using element mapping method. Figure 2b–f show a good distribution of C, N, Ba, Ti and O elements in selected area with a higher contribution of Ba and Ti compared to C and N, which illustrates the higher mass percentage of $BaTiO_3$ than that of g-C_3N_4.

XPS analysis for determination on chemical state of elements consisted in the CN/BTO-200 composite was conducted and the obtained results are presented in figure 3. The high-resolution C1s XPS spectrum clearly shows two peaks at 284.51 and 287.55 eV corresponding to sp^2-hybridized graphitic (C–C) from the adventitious carbon of the instrument background and tri-*s*-triazine carbon (N–C=N) in g-C_3N_4, respectively [17,31]. Compared with the pure g-C_3N_4 [31], the peak of N−C=N in CN/BTO-200 shifts to lower binding energy. The bonding between C and N in the g-C_3N_4 present in CN/BTO-200 was further clarified in the N1s XPS spectrum which could be deconvoluted into three components at 398.55, 399.85 and 401.03 eV corresponding to Nsp^2 (C–N=C), ternary-N (N–$(C)_3$) and primary C–N–H, respectively. These data are consistent with the g-C_3N_4 structure reported in previous publication [31–33]. The Ba3d spectrum can be deconvoluted into two peaks of $Ba3d_{5/2}$ at 778.65 eV and $Ba3d_{3/2}$ at 794.01 eV, while the high-resolution Ti2p XPS spectrum shows two peaks of $Ti2p_{3/2}$ at 458.65 eV and $Ti2p_{1/2}$ at 464.80 eV. Besides, the O1s XPS spectrum shows one peak at 530.60 eV. These signals are attributed to Ba^{2+}, Ti^{4+} and O^{2-} in $BaTiO_3$ [34]. However, it is worth to note that compared with the pure $BaTiO_3$ [18], the peaks of Ba3d and Ti2p in CN/BTO-200 shifts to lower binding energy. These obtained peak shifts may come from interfacial interactions between g-C_3N_4 and $BaTiO_3$ in the composite. Furthermore, the lower peak shifts of Ba3d and Ti2p in CN/BTO-200 could indicate charge transfer rule i.e., electrons transfer from g-C_3N_4 to $BaTiO_3$ in CN/BTO-200 [18].

To investigate the light harvesting properties of the samples, UV–Vis DRS was performed and the spectra are displayed in figure 4a. It is seen that CN and BTO-200 exhibit absorption edges of ~460 and ~390 nm, corresponding to band gap energies of ~2.7 and ~3.2 eV, respectively. For the composite CN/BTO-200, it exhibits an absorption edge of ~420 nm, corresponding to a band gap of ~2.9 eV. The band gap of CN, BTO-200 and CN/BTO-200 were calculated based on UV–Vis DRS spectra using the Kubelka–Munk equation [35] as shown in figure 4b–d. Accordingly, the band gap energy of CN, BOT and CN/BTO-200 are 2.7, 3.2 and 2.9 eV, respectively, which are in accordance with the report [29].

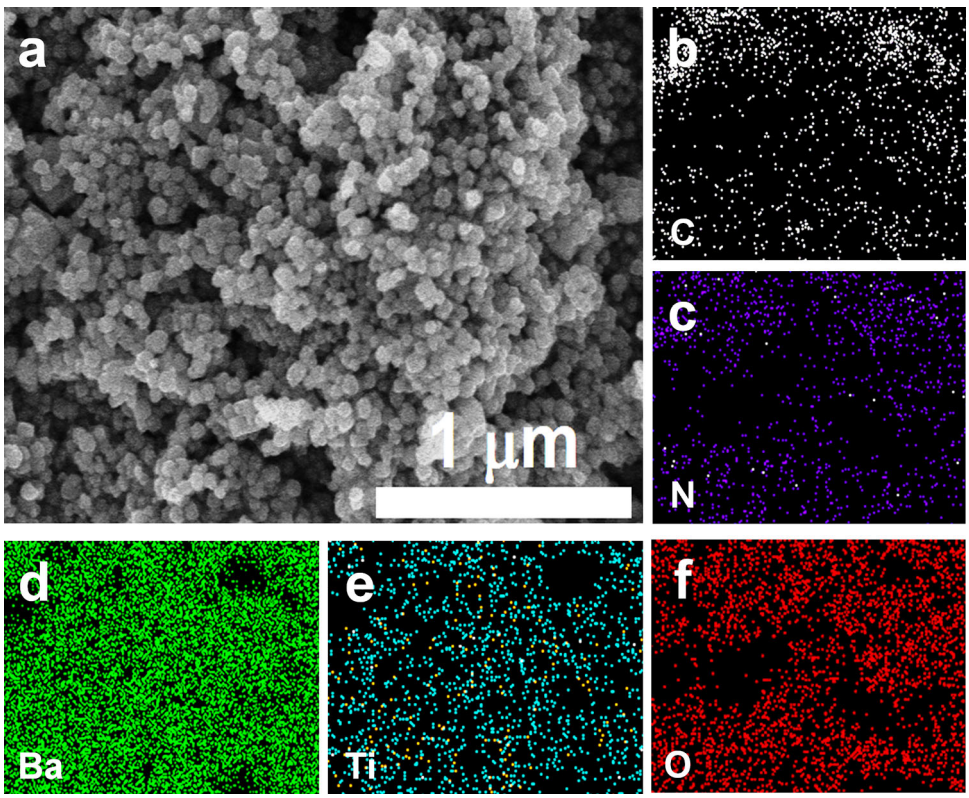

Figure 2. (**a**) SEM image and (**b–f**) EDS mapping images of C, N, Ba, Ti and O for CN/BTO-200.

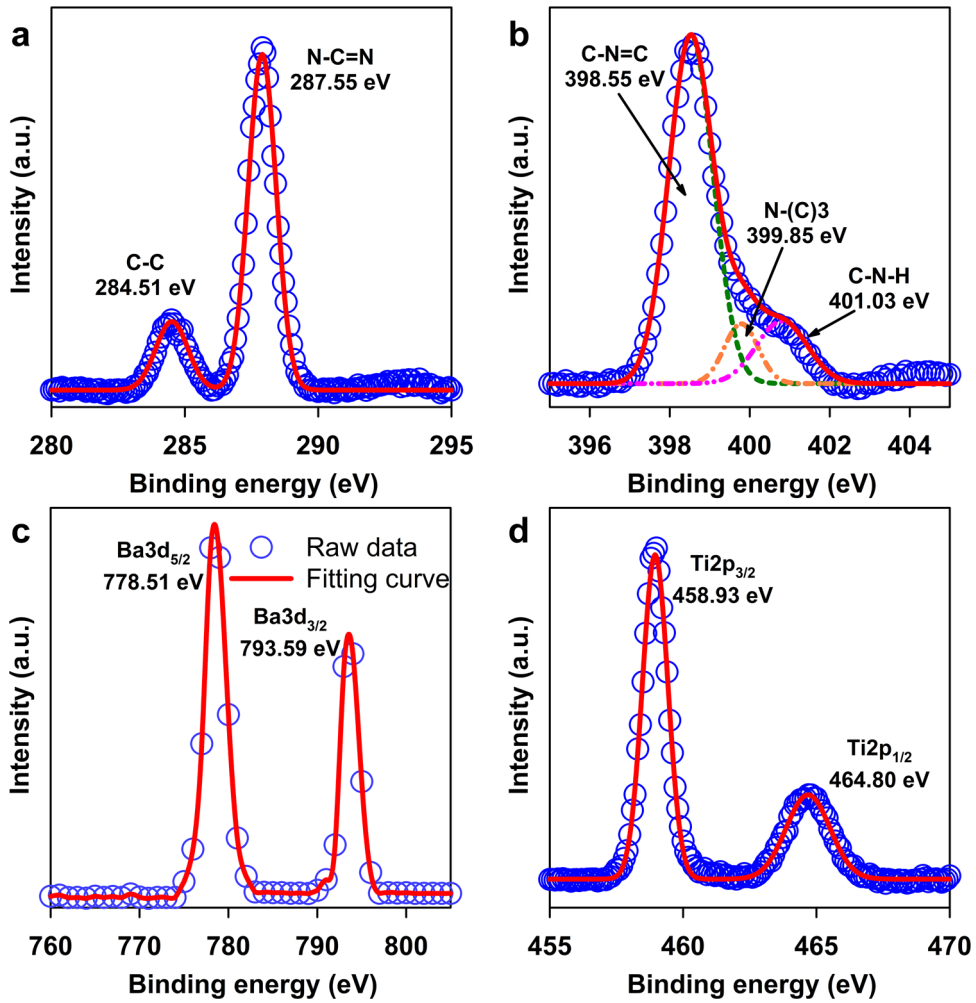

Figure 3. XPS spectra of (**a**) C1s, (**b**) N1s, (**c**) Ba3d and (**d**) Ti2p for CN/BTO-200.

Figure 5a shows the photocatalytic degradation of MB over CN, BTO-200 and CN/BTO-200 as a function of irradiation time. After 7 h of irradiation, the decomposition efficiency of MB in case of composite CN/BTO-200 reaches to 98.72% which is much higher than BTO-200 (28.90%) and CN (41.31%). This result demonstrates that composite of $BaTiO_3$ and g-C_3N_4 performs superior photocatalytic activity compared to single components which could be explained by a synergic effect between them to reduce the high-rate recombination of photogenerated electron–hole pairs, a common disadvantage of pristine semiconductors. Additionally, two g-C_3N_4/$BaTiO_3$ composites with various weight ratios of g-C_3N_4:$BaTiO_3$ to be 0.5:10 and 1.5:10 were investigated, indicating that the decomposition efficiency of the two composites (60.18 and 47.07%, respectively) is better than that of CN and BTO-200, but lower than that of the g-C_3N_4:$BaTiO_3$ composite with weight ratio of g-C_3N_4:$BaTiO_3$ to be 1:10 (CN/BTO-200).

The enhancement in photocatalytic activity was clearly illustrated by the kinetic evaluation result as shown in figure 5b, which is obtained by application of Langmuir–Hinshelwood model via pseudo-first ordered equation (equation (1)) [36]:

$$\ln\frac{C_0}{C} = kKt = k't, \tag{1}$$

where k' is referred as rate constant of MB degradation reaction. The high value of regression coefficient demonstrates that photocatalytic reactions over all samples follow well to the pseudo-first ordered kinetic equation. As indicated in figure 5b, the values of rate constant k' for CN/BTO-200, CN and BTO-200 were calculated to be 10.32×10^{-3}, 1.35×10^{-3} and 1.28×10^{-3}, respectively. Apparently, the rate constant for CN/BTO-200 is around 7.6 and 8.0 times higher than that of CN and BTO-200, respectively. A comparison of the rate constant for CN/BTO-200 with other photocatalysts is shown in table 1. It can be observed that CN/BTO-200 possesses a relatively high rate constant, while we use a light source with the lowest power.

The mechanism of catalytic process and role of free radicals were investigated using quencher to scavenge the active species [37]. In particular, the tert-butyl alcohol (TB), 1,4-benzoquinone (BQ), ammonium oxalate (AO) and dimethyl

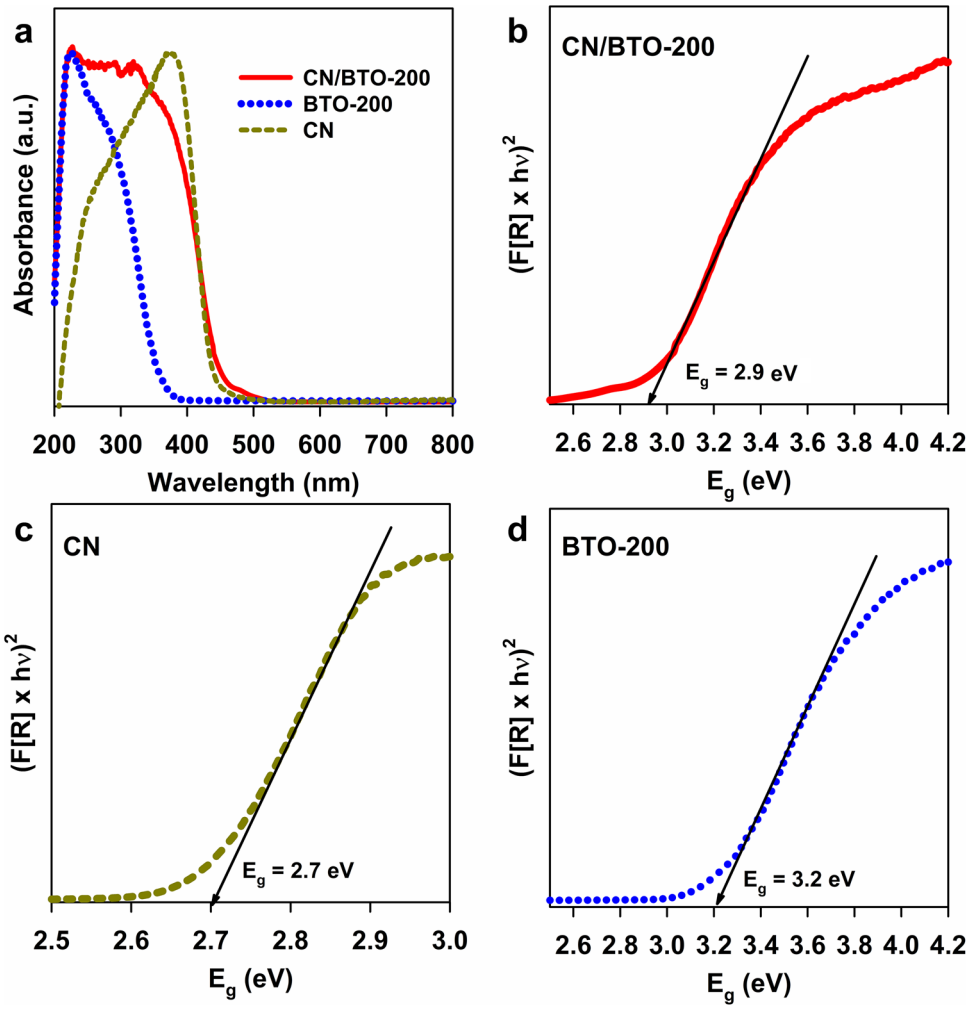

Figure 4. (**a**) UV–Vis–DRS and (**b**, **c** and **d**) band gaps of CN/BTO-200, CN and BTO-200, respectively.

sulphoxide (DMSO) were used as quenchers of $^{\bullet}OH$ [38], $^{\bullet}O_2^-$ [39,40], photo-generated hole [38,39] and photo-induced electrons [37], respectively. All quenching solutions were prepared with a concentration of 1 mmol l^{-1} and added to the testing solution with volume of 2 ml. Figure 5c shows that there is a significant reduction in the presence of quenchers compared to the original experiment. Accordingly, the photocatalytic degradation of MB undergoes a decrease from ~98.72% with no quncher to ~89.46, ~83.94, ~66.80 and ~56.78% corresponding to BQ, AO, TB and DMSO, in which DMSO and TB cause the more significant decrease. This illustrates that the main active species in this mechanism are $^{\bullet}OH$ and photo-induced electrons.

Accordingly, the valence band (VB) and conduction band (CB) potentials of $BaTiO_3$ can be calculated [16] using the following equations:

$$E_{VB} = X - E^e + 0.5E_g,$$

$$E_{CB} = X - E^e - 0.5E_g,$$

where X is the absolute electronegativity of $BaTiO_3$ (defined as the arithmetic mean of the electron affinity and the first ionization of the constituent atoms), approximately to be 5.27 eV, E^e is the energy of free electrons on the hydrogen scale (~4.5 eV), and E_g is the band gap energy of $BaTiO_3$ (3.20 eV), the CB and VB potentials of $BaTiO_3$ are calculated to be −0.83 and +2.37 V *vs.* normal hydrogen electrode (NHE), respectively.

Based on the obtained experimental results, a proposed mechanism toward the degradation of MB on CN/BTO-200 composite is schematically shown in figure 5d. In the composite, due to the more positive potentials of both VB and CB edges of g-C_3N_4 compared to $BaTiO_3$, these semiconductors could form a heterojunction, in which photogenerated electrons could transfer from CB of g-C_3N_4 to CB of $BaTiO_3$, leading to the extension of lifetime of photogenerated charge carriers. This is partially supported from the above XPS data. The electrons on CB of $BaTiO_3$ then reduce adsorbed oxygen to form $^{\bullet}O_2^-$, followed by the multi-electron redox to yield $^{\bullet}OH$. Similarly, the hole on VB of $BaTiO_3$ could transport to VB of g-C_3N_4 through the internal electric field at the interaction area of both components which later directly oxidizes MB. Therefore, all the

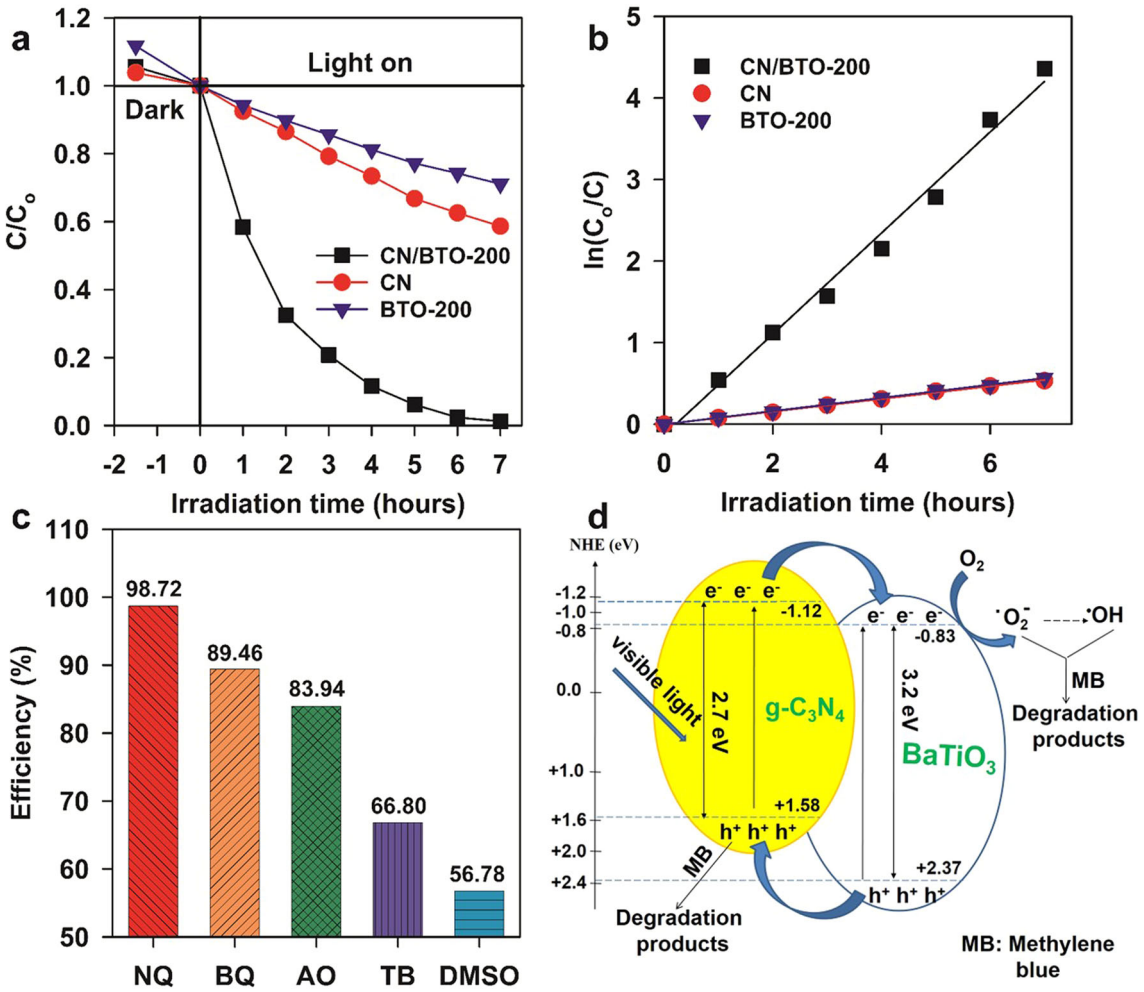

Figure 5. (**a**) Photocatalytic degradation and (**b**) kinetic plots for degradation of MB on CN, BTO-200 and CN/BTO-200 under visible light; (**c**) effect of various quenchers on photodegradation of MB over CN/BTO-200 after 7 irradiation hours under visible light, and (**d**) schematic illustration of electron–hole separation and transport and photocatalytic activity of CN/BTO-200 under visible light irradiation.

Table 1. Comparison of the rate constants of MB photodegradation under visible light for the photocatalyst developed in the present study with other reported photocatalysts.

Photocatalysts	MB dye concentration, mg l^{-1}	Catalyst concentration, mg l^{-1}	Light source (visible light)	k, min^{-1}	References
g-C_3N_4/AgBr/ZnO	5	400	300 w	41.0×10^{-3}	[41]
PTh/ZnO	6.4	1000	250 w	24.239×10^{-3}	[42]
ZnO NPs	100	1000	Solar radiation	8.7×10^{-3}	[43]
g-C_3N_4/$SrTiO_3$	5	200	500 w	7.1×10^{-3}	[44]
g-C_3N_4/$NiTiO_3$	10	200	100 w	0.88×10^{-3}	[45]
Pd-doped NiO/SiO_2	10	500	400 w	0.218×10^{-3}	[46]
g-C_3N_4/$BaTiO_3$	50	500	75 w	10.32×10^{-3}	Present work

active species contribute to the total efficiency of the composite in the degradation of MB. In other words, besides the role of enhancement in the light adsorption as discussed in previous sections, heterojunction between $BaTiO_3$ and g-C_3N_4 also provide an effective moving path for photoinduced charge carriers to expand the seperation time of them.

All the aforementioned processes could be summarized in the following equations:

$$\text{g-}C_3N_4/BaTiO_3 \xrightarrow{hv} h^+_{VB}(\text{g-}C_3N_4)/\,e^-_{CB}(BaTiO_3),$$

$$e^- + O_2 \rightarrow {}^\bullet O_2^-,$$

$${}^\bullet O_2^- + H^+ \rightarrow {}^\bullet OOH,$$

$${}^\bullet OOH + H^+ + e^- \rightarrow H_2O_2,$$

$$H_2O_2 + e^- \rightarrow {}^\bullet OH + OH^-,$$

$$H_2O_2 + {}^\bullet O_2^- \rightarrow {}^\bullet OH + OH^- + O_2,$$

$${}^\bullet OH, {}^\bullet O_2^-, h^+ + MB \rightarrow \text{degradation products}.$$

4. Conclusion

In this work, for the preparation of $BaTiO_3$ precusor, reaction temperature at 200°C is better than those of 180 and 220°C. Using the as-prepared $BaTiO_3$, $BaTiO_3$/g-C_3N_4 composite was prepared via a facile hydrothemal method from the two components, $BaTiO_3$ and g-C_3N_4. The photocatalytic rate of MB degradation for the composite is 7.6 and 8.0 times higher than that of CN and BTO-200, respectively, which is due to a synergic effect between two components in reduction of photogenerated electron–hole recombination. A mechanism was also proposed based on the heterojunction model from the two semiconductor components.

Acknowledgement

This work was financially supported by the Vietnam Ministry of Education and Training (Grant No. B2019-DQN-12).

References

[1] Chan S H S, Wu T Y, Juan J C and Teh C Y 2011 *J. Chem. Technol. Biotechnol.*, https://doi.org/10.1002/jctb.2636
[2] Rauf M A and Ashraf S S 2009 *J. Hazard. Mater.*, https://doi.org/10.1016/j.jhazmat.2008.11.043
[3] Lee W W, Chung W H, Huang W S, Lin W C, Lin W Y, Jiang Y R *et al* 2013 *J. Taiwan Inst. Chem. Eng.*, https://doi.org/10.1016/j.jtice.2013.01.005
[4] Robinson T, McMullan G, Marchant R and Nigam P 2001 *Biores. Technol.*, https://doi.org/10.1016/S0960-8524(00)00080-8
[5] Bora L V and Mewada R K 2017 *Renew. Sust. Energ. Rev.*, https://doi.org/10.1016/j.rser.2017.01.130
[6] Byrne C, Subramanian G and Pillai S C 2018 *J. Environ. Chem. Eng.*, https://doi.org/10.1016/j.jece.2017.07.080
[7] Gupta S M and Tripathi M 2011 *Chin. Sci. Bull.*, https://doi.org/10.1007/s11434-011-4476-1
[8] Lee K M, Lai C W, Ngai K S and Juan J C 2016 *Water Res.*, https://doi.org/10.1016/j.watres.2015.09.045
[9] Dong P, Hou G, Xi X, Shao R and Dong F 2017 *Environ. Sci. Nano*, https://doi.org/10.1039/C6EN00478D
[10] Peña M A and Fierro J L G 2001 *Chem. Rev.*, https://doi.org/10.1021/cr980129f
[11] Yan Y, Yang H, Yi Z, Li R and Wang X 2019 *Micromachines*, https://doi.org/10.3390/mi10040254
[12] Ha M N, Zhu F, Liu Z, Wang L, Liu L, Lu G *et al* 2016 *RSC Adv.*, https://doi.org/10.1039/C6RA03472A
[13] Devi L G and Nithya P M 2018 *Inorg. Chem. Front.*, https://doi.org/10.1039/C7QI00590C
[14] Nageri M, Shalet A B and Kumar V 2017 *J. Mater. Sci.: Mater. Electron.*, https://doi.org/10.1007/s10854-017-6729-5
[15] Yongfei Cui, Joe Brisco, Yaqiong Wang, Nadezda V Tarakina and Steve Dunn 2017 *ACS Appl. Mater. Interfaces*, https://doi.org/10.1021/acsami.7b03523
[16] Xian T, Yang H, Di L J and Dai J F 2015 *J. Alloys Compd.*, https://doi.org/10.1016/j.jallcom.2014.11.051
[17] Yang B, Wu C, Wang J, Bian J, Wang L, Liu M *et al* 2020 *Ceram. Int.*, https://doi.org/10.1016/j.ceramint.2019.10.145
[18] Wu M, Ding T, Wang Y, Zhao W, Xian H, Tian Y *et al* 2019 *Catal. Today*, https://doi.org/10.1016/j.cattod.2019.04.061
[19] Kroke E and Schwarz M 2004 *Coord. Chem. Rev.*, https://doi.org/10.1016/j.ccr.2004.02.001
[20] Goglio G, Foy D and Demazeau G 2008 *Mater. Sci. Eng.: R: Rep.*, https://doi.org/10.1016/j.mser.2007.10.001
[21] Chen X, Zhang J, Fu X, Antonietti M and Wang X 2009 *J. Am. Chem. Soc.*, https://doi.org/10.1021/ja903923s
[22] Marth S, Nashim A and Parid K M 2013 *J. Mater. Chem. A*, https://doi.org/10.1039/C3TA10851A
[23] Yongfei C, Joe B and Steve D 2013 *Chem. Mater.*, https://doi.org/10.1021/cm402092f
[24] Li J, Inukai K, Tsuruta A, Takahashi Y and Shin W 2017 *J. Asian Ceram. Soc.*, https://doi.org/10.1016/j.jascer.2017.09.006
[25] Scherrer P and Göttinger N 1918 *Math. Phys.* **2** 98
[26] Wang X, Maeda K, Thomas A, Takanabe K, Xin G, Carlsson J M *et al* 2009 *Nat. Mater.*, https://doi.org/10.1038/nmat2317
[27] Yan S C, Li Z S and Zou Z G 2009 *Langmuir*, https://doi.org/10.1021/la900923z
[28] Ni Y, Zheng H, Xiang N, Yuan K and Hong J 2015 *RSC Adv.*, https://doi.org/10.1039/C4RA13642J
[29] Kappadan S, Gebreab T W, Thomas S and Kalarikkal N 2016 *Mater. Sci. Semicond. Process.*, https://doi.org/10.1016/j.mssp.2016.04.019
[30] Wang P, Fan C, Wang Y, Ding G and Yuan P 2013 *Mater. Res. Bull.*, https://doi.org/10.1016/j.materresbull.2012.11.075
[31] Ji C, Yin S N, Sun S and Yang S 2018 *Appl. Surf. Sci.*, https://doi.org/10.1016/j.apsusc.2017.11.233
[32] Li J, Liu E, Ma Y, Hu X, Wan J, Sun L *et al* 2016 *Appl. Surf. Sci.*, https://doi.org/10.1016/j.apsusc.2015.12.236
[33] Liu E, Chen J, Ma Y, Feng J, Jia J, Fan J *et al* 2018 *J. Colloid Interface Sci.*, https://doi.org/10.1016/j.jcis.2018.04.038
[34] Nayak S, Sahoo B, Chaki T K and Khastgir D 2014 *RSC Adv.*, https://doi.org/10.1039/C3RA44815K
[35] Rauf A, Shah M A S, Lee J Y, Chung C H, Bae J W and Yoo P J 2017 *RSC Adv.*, https://doi.org/10.1039/C7RA03854B
[36] Xiao X, Hu R, Liu C, Xing C, Qian C, Zuo X *et al* 2013 *Appl. Catal. B: Environ.*, https://doi.org/10.1016/j.apcatb.2013.04.037
[37] Shi L, Liang L, Ma J, Wang F and Sun J 2014 *Dalton Trans.*, https://doi.org/10.1039/C4DT00087K
[38] Lim J, Kim H, Alvarez P J J, Lee J and Choi W 2016 *Environ. Sci. Technol.*, https://doi.org/10.1021/acs.est.6b03250

[39] Shi L, Liang L, Ma J, Wang F and Sun J 2014 *Catal. Sci. Technol.*, https://doi.org/10.1039/C3CY00871A
[40] Ghugal S G, Umare S S and Sasikala R 2015 *RSC Adv.*, https://doi.org/10.1039/C5RA09974A
[41] Elham B A, Alireza B and Moayad H S 2018 *J. Phys. Chem. Solids,* https://doi.org/10.1016/j.jpcs.2018.06.024
[42] Faisal M, Farid A H, Mohammed J, Alsaiari M A, Al-Sayari S A and Al-Assiri M S 2020 *Mater. Today Commun*., https://doi.org/10.1016/j.mtcomm.2020.101048
[43] Morteza G, Moones H and Saeed G 2020 *Spectrochim. Acta Part A: Molec. Biomolec. Spectrosc.*, https://doi.org/10.1016/j.saa.2019.117961
[44] Panagiotis S K, Ioannis K, Dimitrios P and Triantafyllos A 2018 *Catalysts*, https://doi.org/10.3390/catal8110554
[45] Thanh T P and Eun W S 2020 *Appl. Surf. Sci*., https://doi.org/10.1016/j.apsusc.2019.143992
[46] Mohamed R M and Harraz F A 2020 *Mater. Res. Bull.,* https://doi.org/10.1016/j.materresbull.2020.110965